IEEE Access
Multidisciplinary | Rapid Review | Open Access Journal

Received June 17, 2019, accepted June 30, 2019, date of publication July 8, 2019, date of current version July 26, 2019.

Digital Object Identifier 10.1109/ACCESS.2019.2927259

A Novel Fully Reconfigurable Non Foster Capacitance Using Distributed Negative Group Delay Networks

TIEDI ZHANG AND TAO YANG, (Senior Member, IEEE)
School of Electronic Science and Engineering, University of Electronic Science and Technology of China, Chengdu 611731, China
Department of Electronic Science and Engineering, University of Electronic Science and Technology of China, Chengdu 611731, China

Corresponding author: Tao Yang (yangtao8314@uestc.edu.cn)

This work was supported in part by the NSFC under Grant 61801103, and in part by the National Key Project of Science and Technology.

ABSTRACT A novel reconfigurable non-Foster capacitance (NFC) using negative group delay (NGD) circuit is presented in this paper. The NGD circuit is based on a multi-order distributed amplifier which is used to achieve both NGD performance and gain compensation. By introducing shunt and series varactors next to trans-conductance transistors in the amplifier, the characteristic impedance, and electric length of transmission lines in the distributed amplifier can be flexibly tuned. As a result, the gain, phase shift, and negative group delay value of the proposed NGD circuit can be easily controlled as desired, and therefore, the scattering parameters S_{21} can be adjusted to match with an ideal NFC, resulting in reconfigurable non-Foster capacitance. The working frequency ranges, equivalent negative capacitance value, and connection modes of the NFC be fully reconfigured by appropriately controlling the voltages applied to the varactors. Both simulation and measurement results were given, which agree well with each other. The experimental results show that the NFC value can be tuned from −1.1 to −2.5pF with 1 GHz center frequency and the working frequency can be tuned from 0.7 to 0.8 GHz with −10 pF shunt NFC.

INDEX TERMS Reconfigurable non-Foster capacitance, negative group delay, non-Foster reactance.

I. INTRODUCTION

For the wideband signal, the transmission phase is distinct at different frequencies, and this phenomenon is called group delay. Group delay $\tau(\omega)$ is defined as the slope of the phase-frequency curve, namely

$$\tau(\omega) = -\frac{\partial \varphi(\omega)}{\partial \omega} \tag{1}$$

where $\varphi(\omega)$ is the phase-frequency response. For the conventional components, the group delay is usually positive but for an NGD circuit, the group delay is negative.

The NGD concept was firstly investigated by Brillouin in 1960s while observing wave propagation through different media [1]. Since that, NGD circuits have gained much attention and a series of NGD circuits have been investigated [2]–[12]. The negative impedance converter was used to implement reflective type NGD response for extending the bandwidth of antenna in [13]; RLC series/shunt network was proposed as an effective method to build NGD cell, and high order RLC cells were then applied to achieve NGD performance in wider bandwidth with flat gain in [14]; The coupled-line structure was applied to implement wideband NGD response by using two reflection resistors in [15]; Circuits applying directional coupler with resistance loaded at the direct and coupled ports can achieve NGD performance without extra resonators in [16].

With these in-depth researches on NGD circuits, it has been discovered that equivalent non-Foster (NF) reactive elements can be achieved [17] by adjusting the gain and phase response of an NGD circuit. The NF reactive elements have negative values and should satisfy

$$\frac{\partial B_{NF}}{\partial \omega} < 0 \quad \frac{\partial \mathrm{X_{NF}}}{\partial \omega} < 0 \tag{2}$$

where B_{NF} is susceptance and X_{NF} is reactance. The NF reactive elements don't obey Foster's reactance theorem, and thus, they usually work as negative capacitance and inductance.

The circuit using NF reactive elements can break the limitation of Bode-Fano law, which makes it widely used in antenna's impedance matching [18]–[24]. Typically, NF reactive elements include the non-Foster capacitor (NFC)

The associate editor coordinating the review of this manuscript and approving it for publication was Wenjie Feng.

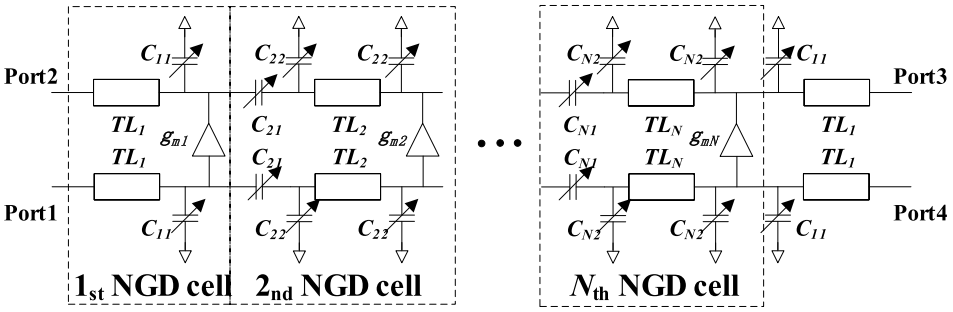

FIGURE 1. Schematic of the proposed reconfigurable N^{th}-order NFC circuit.

with negative capacitance and the non-Foster inductor with negative inductance. Among these two types of NF reactive elements, NFC circuits have been used in a variety of applications to improve system performance. For examples, in [25], a varactor shunt with NFC has been proposed with wider tuning range as compared to the traditional one; in [26], the NFC helped the amplifier to achieve a wider bandwidth impedance matching; in [27], the NFC can also improve the efficiency of a class-E power; and in [28], an NFC was applied at an electrostatic discharge (ESD) protection unit, making the amplifier working in a wider band. Even though NFC has been used in many aforementioned applications, it needs to be noted that most of these NFCs were implemented by using lumped components [29], which caused large parasitic parameters at high frequency and limited its application. Moreover, the obtained capacitance using lumped components cannot be adjusted flexibly and only affords fixed working frequency and connection type. In [30] and [31], reconfigurable NFC and matching network are implemented with distributed amplifier structure, however, only the capacitance value was tunable by that structure, restricting the circuit's application.

In this paper, a novel reconfigurable NFC structure has been proposed based on the distributed NGD circuit. By loading series and shunt varactors in the transmission sections, reconfigurable transmission coefficients that are equivalent to an ideal NFC circuit can be obtained. The resulted NFC can be fully reconfigurable either simultaneously or separately in terms of capacitance value, working frequency and connection types. Additionally, the extra NGD cells can be added to extend the bandwidth.

II. THE PRINCIPLE OF EQUIVALENT NON FOSTER CAPACITANCE USING DISTRIBUTED NGD CIRCUIT

Fig. 1 shows the schematic of proposed reconfigurable NFC circuit. It consists of an N^{th} order distributed amplifier with varactors. Port 1 is served as the input port, while Port 2 is the output port. Port3 and Port 4 are dummy ports and are connected to 50 Ω terminals. The transmission sections from Port 2 to 3 are symmetrical to the ones from Port 1 to 4 with respect to the trans-conductance transistors in between. The first NGD cell is composed by a transmission line TL_1, a shunt varactor C_{11} and a transconductance transistor g_{m1}. For the K^{th} NGD cell ($2 \leq K \leq N$), it consists of a transmission line TL_K, a series varactor C_{K1}, two shunt varactors C_{K2} with same value and a transconductance g_{mK}. The last transmission section next Port 3 or Port 4 consists of a transmission line TL_1 and a shunt varactor C_{11}, which have same values as in the first NGD cell. All transconductances have the same value, namely, $g_{m1} = g_{mK} = g_0$. To achieve the equivalent NFC, the order of the circuit should be greater than or equal to 2.

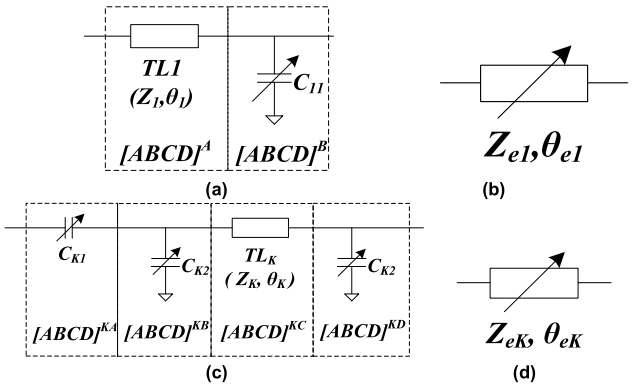

FIGURE 2. (a) Transmission section of the first NGD cell and (b) its equivalent circuit. (c) Transmission section of the K^{th} NGD cell and (d) its equivalent circuit.

The transmission section of the first NGD cell is shown in Fig. 2(a), and it is constructed by a fixed-length transmission line section and a shunt varactor. By tuning the shunt varactor, this transmission section can be equivalent to a reconfigurable transmission line with effective characteristic impedance Z_{e1} and electric length θ_{e1}, as shown in Fig. 2(b). The [ABCD] matrix of the transmission section in the first NGD cell can be calculated as

$$\begin{bmatrix} A & B \\ C & D \end{bmatrix} = \begin{bmatrix} \cos\theta_1 & jZ_1 \sin\theta_1 \\ \dfrac{j\sin\theta_1}{Z_1} & \cos\theta_1 \end{bmatrix} \begin{bmatrix} 1 & 0 \\ j\omega C_{11} & 1 \end{bmatrix} \quad (3)$$

where Z_1 and θ_1 are characteristic impedance and phase of TL_1. S_{21} can be derivate from (3) as in (4), as shown at the top of the next page,

$$S_{21} = \frac{2}{2\cos\theta_1 - Z_1\omega C_{11}\sin\theta_1 + j\left(\frac{Z_1}{Z_0}\sin\theta_1 + \frac{Z_0}{Z_1}\sin\theta_1 + \omega C_{11}Z_0\cos\theta_1\right)} \tag{4}$$

For the transmission line with characteristic impedance Z_{e1} and phase θ_{e1} in Fig. 2(b), S_{21} can be calculated as

$$S_{21} = \frac{2}{2\cos\theta_{e1} + j\sin\theta_{e1}\left(\frac{Z_0}{Z_{e1}} + \frac{Z_{e1}}{Z_0}\right)} \tag{5}$$

Making (4) equal to (5) in both real and imaginary part, the transmission section of the first NGD cell can be equivalent to the transmission line in Fig. 2(b). The equivalent characteristic impedance Z_{e1} and electric length θ_{e1} can be calculated as,

$$\theta_{e1} = \arccos\left(\cos\theta_1 - \frac{1}{2}Z_1\omega C_{11}\sin\theta_1\right) \tag{6}$$

$$Z_{e1} = \frac{X_1 Z_0 + \sqrt{X_1^2 Z_0^2 - 4Z_0^2}}{2} \tag{7}$$

where

$$X_1 = \frac{\left(\frac{Z_1}{Z_0} + \frac{Z_0}{Z_1}\right)\sin\theta_1 + \omega C_{11}Z_0\cos\theta_1}{\sin\theta_{e1}} \tag{8}$$

The existing conditions are

$$-1 \le \cos\theta_1 - \frac{1}{2}Z_1\omega C_{11}\sin\theta_1 \le 1 \tag{9}$$

$$X_1^2 - 4 \ge 0 \tag{10}$$

From (6) and (7), it can be easily found that the Z_{e1} and θ_{e1} of the equivalent transmission line can be controlled and tuned by $C_{11,}$ resulting in a reconfigurable transmission line section. Z_{e1} is proportional to X_1, The minimum value of Z_{e1} is when $X_1 = 2$.

The transmission section of the K^{th} NGD cell ($2 \le K \le N$) in Fig. 2(c) can be also equivalent to a reconfigurable transmission line with effective characteristic impedance Z_{eK} and effective electric length θ_{eK} as given in Fig. 2(d). The transfer matrix of the transmission sections in the K^{th} NGD cell can be calculated as:

$$\begin{bmatrix} A & B \\ C & D \end{bmatrix} = \begin{bmatrix} 1 & \frac{1}{j\omega C_{K1}} \\ 0 & 1 \end{bmatrix}\begin{bmatrix} 1 & 0 \\ j\omega C_{K2} & 1 \end{bmatrix} \times \begin{bmatrix} \cos\theta_K & jZ_K\sin\theta_K \\ \frac{j\sin\theta_K}{Z_K} & \cos\theta_K \end{bmatrix}\begin{bmatrix} 1 & 0 \\ j\omega C_{K2} & 1 \end{bmatrix} \tag{11}$$

From (11), S_{21} of the transmission sections in the K^{th} NGD cell can be calculated as,

$$S_{21} = \frac{2}{X_{REK} + jX_{MMK}} \tag{12}$$

where

$$X_{REK} = 2\left(1 + \frac{C_{K2}}{C_{K1}}\right)\cos\theta_K + \left(\frac{1}{Z_K\omega C_{K1}} - 2Z_K\omega C_{K2} - \frac{Z_K\omega C_{K2}^2}{C_{K1}}\right)\sin\theta_K \tag{13}$$

$$X_{IMK} = \frac{Z_k}{Z_0}\left(1 + \frac{C_{K2}}{C_{K1}} + \frac{Z_0^2}{Z_k^2} - Z_0^2\omega^2 C_{K2}^2\right)\sin\theta_k + \left(2Z_0\omega C_{K2} - \frac{1}{\omega C_{K1}Z_0}\right)\cos\theta_k \tag{14}$$

Similarly, S_{21} of the equivalent transmission line in Fig. 2(d) can be obtained in the form of (5) with equivalent characteristic impedance Z_{eK} and phase θ_{eK}. By comparing (12) and (5), the equivalent relation between Fig.2(c) and (d) can be calculated as,

$$\theta_{eK} = \arccos\left(\frac{1}{2}X_{REK}\right) \tag{15}$$

$$Z_{eK} = \frac{Z_0}{2}\left\{X_{INK}/\sin\left[\arccos\left(\frac{1}{2}X_{REK}\right)\right] + \sqrt{X_{IMK}^2/\sin^2\left[\arccos\left(\frac{1}{2}X_{REK}\right)\right] - 4}\right\} \tag{16}$$

where X_{REK} and X_{IMK} are given in (13) and (14). For (15) and (16), the existing conditions are

$$-1 \le \frac{1}{2}X_{REK} \le 1 \tag{17}$$

$$X_{IMK}^2/\sin^2\left[\arccos(\frac{1}{2}X_{REK})\right] - 4 \ge 0 \tag{18}$$

The minimum value of Z_{eK} is achieved when (18) equals to 0. For proof of concept, a numerical study has been taken based on (6) (7) (15) and (16) to demonstrate the equivalent relationship between the proposed NGD transmission sections and its equivalent transmission lines. Fig. 3(a) and (b) shows the comparison of real and imaginary part of S_{21}, respectively, between the reconfigurable transmission sections in the first NGD cell with different C_{11} and the corresponding equivalent transmission lines. As can be observed, by varying C_{11}, the transmission sections in the first NGD cell can be reconfigured to be transmission lines with different characteristic impedance and electric length. Fig. 3(c) and (d) shows the comparison of real and imaginary part of S_{21}, respectively, between the reconfigurable transmission line sections in the K^{th} NGD cell with different C_{K1} and C_{K2} and the corresponding ideal transmission lines. Again, by varying C_{K1} and C_{K2}, the transmission sections in the K^{th} NGD cell can be reconfigured to be different transmission lines with different characteristic impedance and electric length.

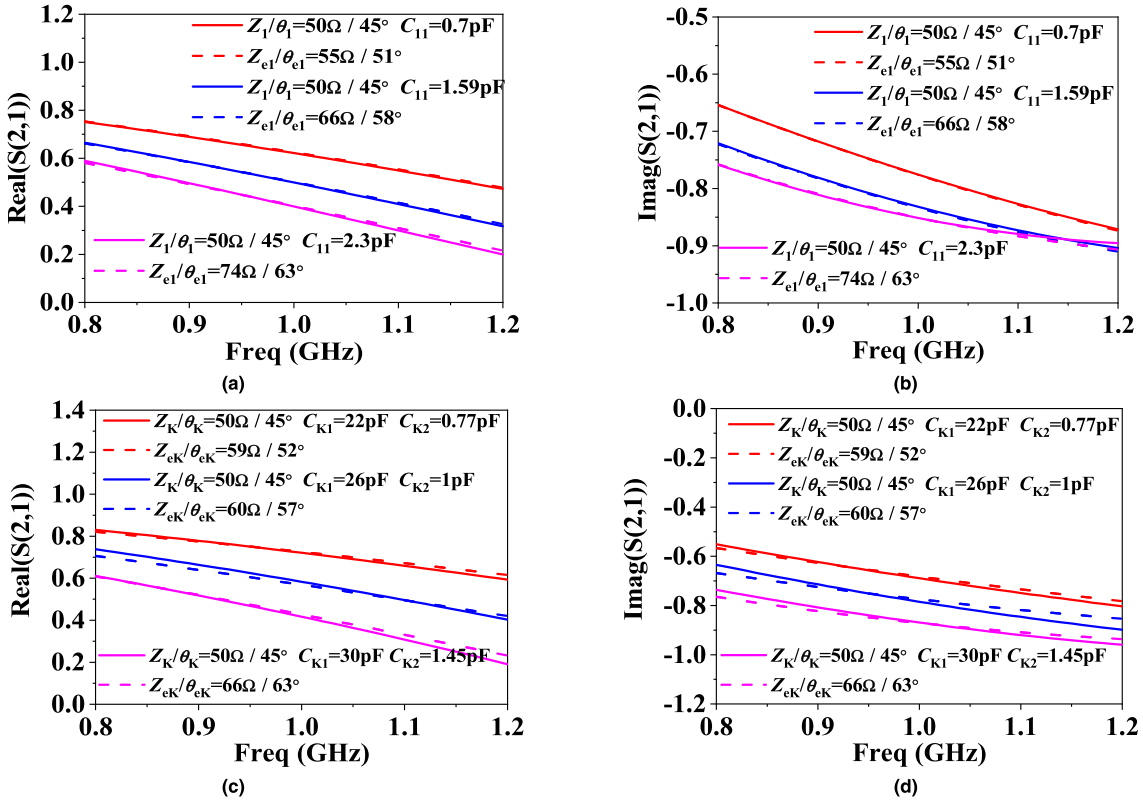

FIGURE 3. (a) Real part and (b) imaginary part of S_{21} of the transmission sections in the first NGD cell and its corresponding ideal transmission lines; (c) Real part and (d) imaginary part of S_{21} of the transmission sections in the K^{th} NGD cells and its corresponding ideal transmission lines.

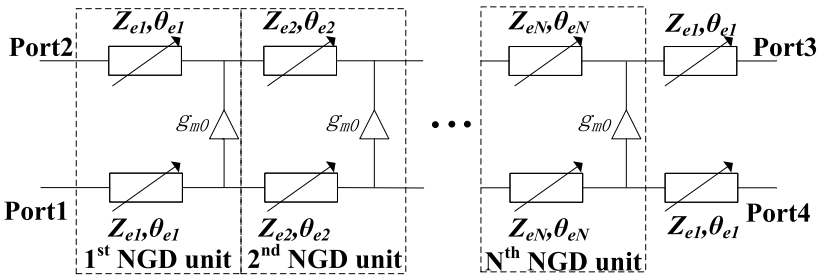

FIGURE 4. Equivalent NFC using reconfigurable lines.

From the theory above, the circuit in Fig. 1 can be equivalent to the one given in Fig. 4. According to [32], the transfer function of the proposed circuit in Fig. 4 can be calculated as

$$H_{NGD}(\omega) = \sum_{k=1}^{N} G_K \exp\left(-j \sum_{i=1}^{K} 2\omega\tau_i\right) \tag{19}$$

where G_K and τ_i are the voltage gain and group delay of the K^{th} NGD cell, and their values are related with Z_{eK}, θ_{eK} and trans-conductance g_{m0}[6]. If the proposed circuit in Fig. 4 can be equivalent to a NFC circuit, the transfer function $H_{\text{NGD}}(\omega)$ needs to be equal to the transfer function of an ideal NFC as,

$$|H_{NGD}(\omega = \omega_0)| = |S_{21NFC}(\omega = \omega_0)| \tag{20}$$

$$\angle H_{NGD}(\omega = \omega_0) = \angle S_{21NFC}(\omega = \omega_0) \tag{21}$$

$$-\frac{\partial \angle H_{NGD}(\omega)}{\partial \omega}\Big|_{\omega=\omega_0} = \tau_{NFC}(\omega = \omega_0) \tag{22}$$

where $|S_{21\text{NFC}}|$ and $\angle S_{21\text{NFC}}$ are the amplitude and phase of S_{21} of the desired NFC, respectively; τ_{NFC} is the group delay of the NFC. In this equivalent circuit, there are totally $2N$-1 unknown parameters (Z_{e1},Z_{e2},...Z_{eN}) and (θ_{e2}, θ_{e3},...θ_{eN}). Note that θ_{e1} is not counted as an unknown parameter since it is a function of Z_{e1}, which can be calculated from (6)-(8) by using C_{11}. Thus, it will generally require $2N$-1 sets of equations to solve all $2N$-1 unknown parameters. Since there are only three equations from (20) to (22), addition constrains

FIGURE 5. The NFC with two connection styles (a) shunt NFC (b) series NFC.

are needed to solve the unknown parameters for higher order NFC circuit when N≥3.

Therefore, auxiliary functions are added to solve the unknown parameters and also ensure that the amplitude and phase of transfer function is consistent with the NFC in a wider bandwidth as,

$$\left.\frac{\partial^{n-2}\left|H_{NGD}(\omega)\right|}{\partial\omega^{n-2}}\right|_{\omega=\omega_0} = \left.\frac{\partial^{n-2}\left|S_{21\ NFC}(\omega)\right|}{\partial\omega^{n-2}}\right|_{\omega=c_0} \quad n=3,4\ldots N \tag{23}$$

$$\left.\frac{\partial\angle H_{NGD}^{n-1}(\omega)}{\partial\omega^{n-1}}\right|_{\omega=\omega_0} = \left.\frac{\partial\angle S_{21NFC}^{n-1}(\omega)}{\partial\omega^{n-1}}\right|_{\omega=c_0} \quad n=3,4\ldots N \tag{24}$$

where $S_{21\mathrm{NFC}}(\omega)$ is the response function of the target NFC. (23) and (24) provide two functions for two extra unknown parameters. By this way, all unknown parameters in the equivalent circuit can be solved. Once the unknown parameters are obtained, the required circuit parameters in Fig. 1 can be calculated from (6)-(8), (15) and (16), resulting a desired reconfigurable NFC circuit. A 2nd order NGD circuit is used as an example to demonstrate the working flow. Firstly, the transfer function of the proposed circuit needs to match with the ideal NFC in phase shift, transfer gain and group delay as (20)-(22). The phase shift, gain and group delay of the ideal negative capacitance can be completely determined by the capacitance value, connection style and working frequency.

Taking a shunt negative capacitance $(-C)$ as an example, its phase shift, transmission gain and group delay can be calculated as [13],

$$|S_{21NFC}(\omega)| = \left|\frac{2j}{Z_0\omega C+2j}\right| \tag{25}$$

$$\angle S_{21NFC}(\omega) = \frac{\pi}{2}-\tan^{-1}\left(\frac{2}{Z_0\omega C}\right) \tag{26}$$

$$\tau_{NFC}(\omega) = \frac{-2Z_0C}{Z_0^2\omega^2C^2+4} \tag{27}$$

From (20)-(22) and (25)-(27), the three unknown parameters in the NGD circuit can be easily determined with three sets of equations.

It should be noted that there are generally two types of connection configuration for a given NFC, which are shunt $-C$ and series $-C$, as shown in Fig. 5. The transmission coefficient for a shunt $-C$ is given in (25)-(27), while the transmission coefficient and group delay for a series $-C$ is given as

$$|S_{21NFC}(\omega)| = \left|\frac{2Z_0\omega C}{2Z_0\omega C+j}\right| \tag{28}$$

$$\angle S_{21NFC}(\omega) = -\tan^{-1}\left(\frac{1}{2Z_0\omega C}\right) \tag{29}$$

$$\tau_{NFC}(\omega) = \frac{-2Z_0C}{4Z_0^2\omega^2C^2+1} \tag{30}$$

As can be seen from (28) and (29), one can notice that the transmission phase of shunt NFC is positive while the transmission phase of series NFC is negative. Since the magnitude of S_{21} for both shunt and series NFC is only determined by the absolute capacitance value of the NFC, thus, if the transmission phase of the proposed NGD circuit can be shifted from negative to positive, the connection types of the given NFC can change from series to shunt, and vice versa.

Once the NGD circuit's S-parameter can match with an NFC, the capacitance value and Q factor can be calculated:

$$C_{NFshunt} = -\frac{1}{\omega\cdot imag(Z_{NFshunt})} \tag{31}$$

where

$$Z_{NFshunt} = \frac{Z_0S_{21}}{2\,(1-S_{21})} \tag{32}$$

and

$$C_{NFseries} = -\frac{1}{\omega\cdot imag(Z_{NFseries})} \tag{33}$$

where

$$Z_{NFseries}=2Z_0\frac{1-S_{21}}{S_{21}} \tag{34}$$

The Q factor can be calculated by

$$Q = \left|\frac{imag\,(Z_{NFshunt})}{real\,(Z_{NFshunt})}\right| Q = \left|\frac{imag\,(Z_{NFseries})}{real\,(Z_{NFseries})}\right| \tag{35}$$

Numeric study based on above theory is taken to demonstrate the 2nd order NGD circuit. The circuit parameters used in simulation and the simulation results are shown in Table 1 and Fig. 6, respectively.

Fig. 6(a) and (b) shows the amplitude and phase, respectively, of S_{21} from an ideal NFC and the proposed NGD circuits. As can be seen, S_{21} of the proposed NGD circuit can be tuned to match S_{21}(in terms of both amplitude and phase) of the ideal NFC with fixed negative capacitance value of -10 pF when the center frequency is changed. This indicates that the proposed NGD circuit can be used as an NFC having reconfigurable working frequency. In each working state/frequency, the resultant NFC has a band-width of 200MHz, and the working frequency can continuously cover from 0.8 GHz to 1.2 GHz, corresponding to a tuning range of 40%.

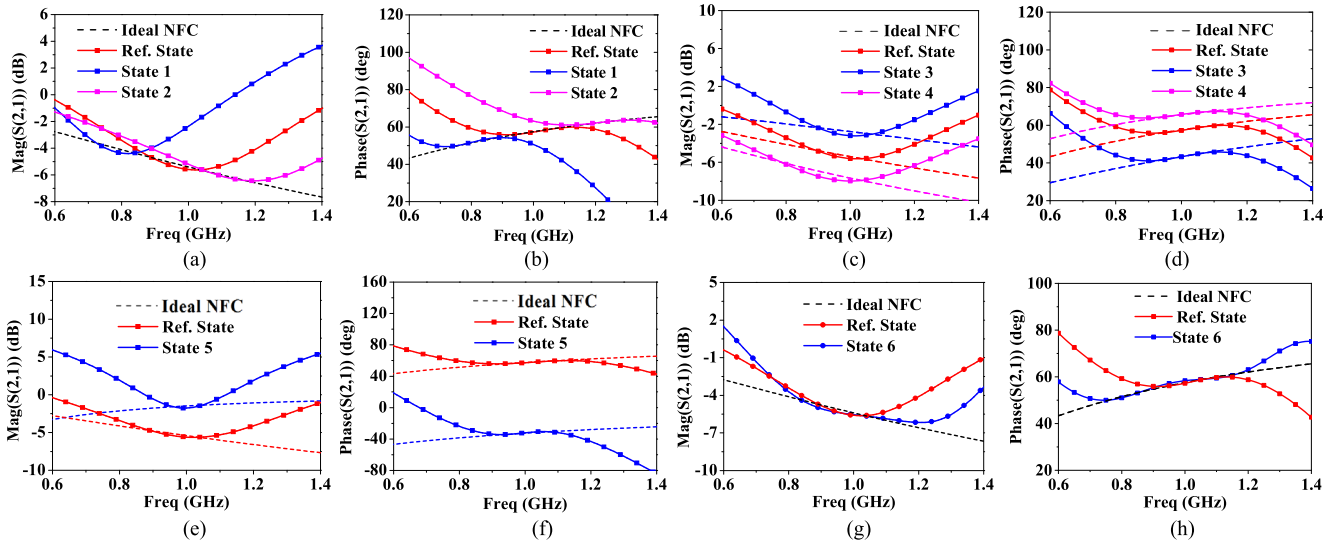

FIGURE 6. Reconfigurable performance of NFC using NG\ D circuit. (a) Amplitude and (b) phase of S_{21} for the proposed NFC circuit at different frequency tuning state. (c) Amplitude and (d) phase of S_{21} for the proposed NFC circuit at different NFC tuning state. (e) Amplitude and (f) phase of S_{21} for the proposed NFC changing from shunt to series connection type. (g) Amplitude and (h) phase of S_{21} for a 2nd order and 3rd order NFC circuit. (Note that Ref. state indicates the initial state of the proposed NFC circuit, and State k (k = 1, 2, 3, 4, 5) indicates the different tuning states of the same NFC circuit.).

TABLE 1. Equivalent NFC using NGD circuit.

	Target NFC	Target center frequency	Connection method	Z_{e1}/θ_{e1}	Z_{e2}/θ_{e2}	Z_{e3}/θ_{e3}	g_m
Ref. State	-10 pF	1 GHz	shunt	50Ω/59.7°	65.7Ω/88°	N/A	31 mS
State 1	-10 pF	0.8 GHz	shunt	48.4Ω/76°	61.6Ω/104.5°	N/A	40 mS
State 2	-10pF	1.2 GHz	shunt	51.9Ω/50.7°	71.5Ω/80.4°	N/A	24 mS
State 3	-6 pF	1 GHz	shunt	48.8Ω/66°	61.7Ω/85.8°	N/A	47 mS
State 4	-14 pF	1 GHz	shunt	49.6Ω/56.7°	65.8Ω/88.6°	N/A	23 mS
State 5	-2.5 pF	1 GHz	series	51Ω/106°	64.2Ω/89°	N/A	62 mS
State 6	-10 pF	1 GHz	shunt	48.1Ω/53.2°	61.3Ω/79.8°	59.3Ω/72.6°	42.3 mS

Fig. 6(c) and (d) shows S_{21} of ideal NFC with three different negative capacitance values and S_{21} of the proposed NFC circuit. It can be found that the NGD circuit can be tuned to match the amplitude and phase of S_{21} of the ideal NFC with different negative capacitance value at given frequency (1 GHz here), respectively. This indicates that the proposed NGD circuit can be used as a NFC having reconfigurable negative capacitance value, and the negative capacitance of the proposed NFC circuit value covers from -14 pF to -6 pF.

Fig. 6(e) and (f) shows S_{21} of the ideal NFC in shunt and series connections, and S_{21} of the proposed NFC circuit. It can be observed that the NGD circuit can be tuned to match the amplitude and phase of S_{21} of the ideal NFC in both shunt and series connection styles. This indicates that the proposed NFC circuit is reconfigurable between shunt and series connections.

Fig. 6(g) and (h) shows amplitude and phase, respectively, of S_{21} with 2nd order (Ref. state) and 3rd order (State 6) NFC circuits. As can be found, the bandwidth of the 3rd order NFC circuits is much wider than the 2nd order NFC circuit, indicating that the proposed NFC circuit can be increased by increasing the NGD cell order.

Fig.7 shows the flow chart of the proposed design. For higher order NFC design, the auxiliary derivative equations can be calculated from (23) and (24), and the same working flow can be used to design the required NFC circuits. The flow chart is an illustration of the adjustable characteristics. In practical design, once the reconfiguration ranges of capacitance value, working frequency and connection mode is determined, the representative central value is usually chosen as the initial value to design transmission line, and then the dynamic adjustment is realized by adjusting the variable capacitor.

III. EXPERIMENTAL RESULTS

To validate the concept, four NFC circuits were fabricated and measured, including a reconfigurable 2nd order NFC circuit in shunt connection mode, a reconfigurable 2nd order NFC circuit in series connection mode, a reconfigurable 2nd order NFC circuit having capability of shunt-to-series transformation, and a reconfigurable 3rd order NFC circuit in shunt connection mode. Commercial software ADS is applied in the design.

TABLE 2. Dimensions and varactors of fabricated circuits.

	w_1(mm)/ $Z_1(\Omega)$	w_2(mm)/ $Z_2(\Omega)$	w_3(mm)/ $Z_3(\Omega)$	l_1(mm)/ $\theta_1(°)$	l_2(mm)/ $\theta_2(°)$	l_3(mm)/ $\theta_3(°)$	C_{11}	C_{21}	C_{22}	C_{31}	C_{32}
C_{2shunt}	0.58/50	0.58/50	N/A	21.5/67	34/105	N/A	SMV1234	SMV1234	SMV1233	N/A	N/A
$C_{2series}$	0.58/50	0.58/50	N/A	32.2/100	19.3/60	N/A	SMV1232	SMV1232	SMV1234	N/A	N/A
C_{SS}	0.58/50	0.58/50	N/A	22.3/69	25.1/78	N/A	SMV1235	SMV1233	SMV1234	N/A	N/A
C_{3shunt}	0.58/50	0.58/50	0.58/50	16.5/51	26.7/83	26.5/82	SMV1233	SMV1233	SMV1235	SMV1234	SMV1234

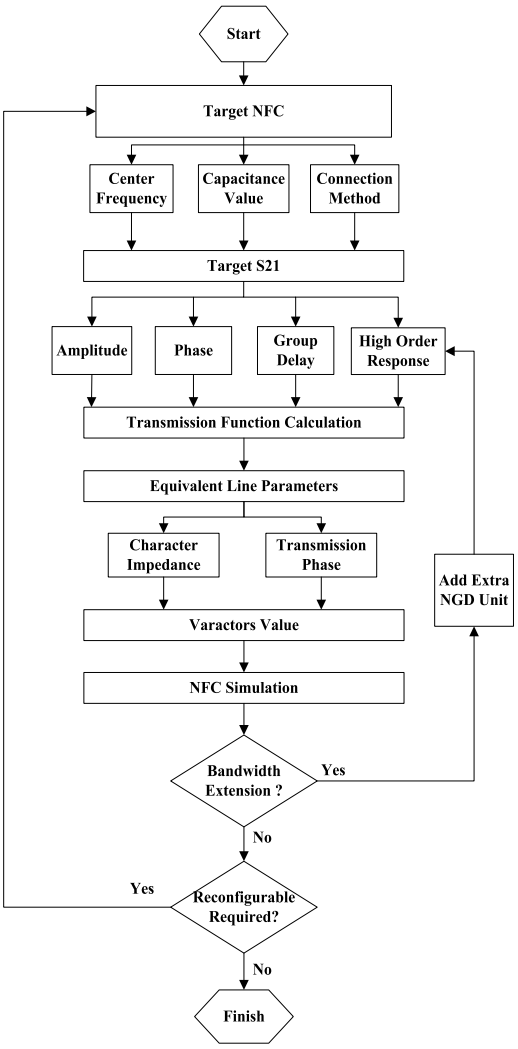

FIGURE 7. The flow chart of the proposed reconfigurable NFC design.

The fabricated circuits are shown in Fig. 8. All circuits are fabricated using 25 mil substrates RO6030 and 2SC5761 transistors from Renesas. The dimension and parameters are shown in Table 2, where w_K and l_K are the width and length of the K^{th} order line, C_{K1} and C_{K2} (K =1,2,3) are varactors. Direct current (DC) block capacitance value and alternating current (AC) block inductance value are given here for simplification. All transistors share the same bias voltage V_{CC} and V_B, ensuring the same g_m for every transistor. At transistor's input port, 0.5 pF series capacitor and

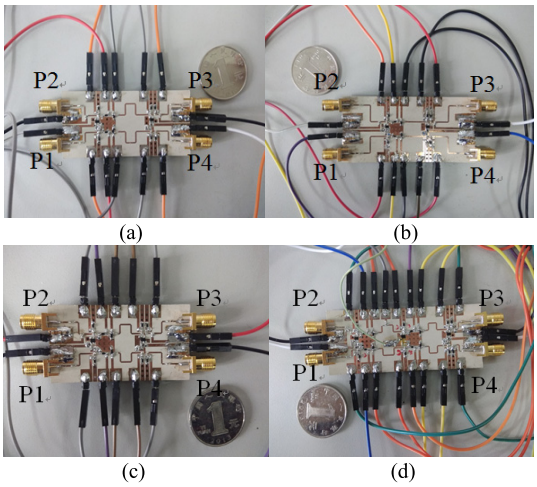

FIGURE 8. Photographs of the reconfigurable (a) 2nd order shunt NFC , (b) 2nd order series NFC, (c) 2nd order NFC with shunt-to-series transformation, and (d) 3rd order shunt NFC.

a network built by shunt 3.9 nH inductor and shunt 3 pF capacitor was set to keep the circuit unconditional stable. The control voltage and DC current for different working conditions are shown in Table 3. The sizes of these four circuits are 54×29.7 mm^2, 63.4×33.7 mm^2, 49.4×29.7 mm^2, 67.7×29.7 mm^2, respectively

A. RECONFIGURABLE 2nd ORDER NFC CIRCUIT IN SHUNT CONNECTION MODE

Fig. 9 shows the simulated and measured results of the reconfigurable 2nd order NFC circuit in shunt connection mode. Simulation agrees well with the measurement. It can be seen that the experimental result is close to the ideal NFC within a 50 MHz bandwidth. By tuning the control voltages on varactors, the center frequency of the NFC can be tuned from 700MHz to 800 MHz with a fixed negative capacitance value of −10 pF, corresponding to a tuning range of 13% which is smaller than the theoretical result in section II. This is due to the limitation of tuning range of the chosen varactors. The equivalent shunt NFCs calculated from S_{21} are shown in Fig. 9(c). The capacitance value error is less than ±0.5 pF in the working bandwidth. The Q factor is larger than 20, as it is shown in Fig. 9(d). The experimental results demonstrate that by using the proposed NGD circuit, a high Q shunt NFC with reconfigurable working frequency can be obtained. Note that

TABLE 3. Voltages of NFC under different conditions.

	V_{11}(V)/ C_{11}(pF)	V_{21}(V)/ C_{21}(pF)	V_{22}(V)/ C_{22}(pF)	V_{31}(V)/ C_{31}(pF)	V_{32}(V)/ C_{32}(pF)	V_B(V)	V_{CC}(V)	I_{DC}(mA)
-10pF 800MHz C_{2shunt}	16.2/1.32	3/3.58	0.7/3.45	N/A	N/A	0.78	1.8	4
-10pF 700MHz C_{2shunt}	0.1/9.63	2.7/3.8	0.2/4.7	N/A	N/A	0.79	1.8	5
-1.1pF 1GHz $C_{2series}$	0.2/4	0.95/2.7	3.9/2.85	N/A	N/A	0.85	1.8	13
-2.5pF 1GHz $C_{2series}$	5.2/1.02	1.4/2.31	1.9/4.8	N/A	N/A	0.84	1.8	11
Shunt C_{ss}	4.3/4.8	1.2/3.1	0.7/7.2	N/A	N/A	0.82	1.8	9
Series C_{ss}	2.6/7.2	2.2/2.3	0.8/7.3	N/A	N/A	0.84	1.8	13
-10pF 800MHz C_{3shunt}	11/0.88	0.4/4.08	4.7/4.3	3.4/3.2	2/4.68	0.77	1.8	2
-3.8pF 900MHz C_{3shunt}	17/0.83	0.76/3.5	18.7/2.35	5.2/2.23	3.9/2.88	0.79	1.8	6

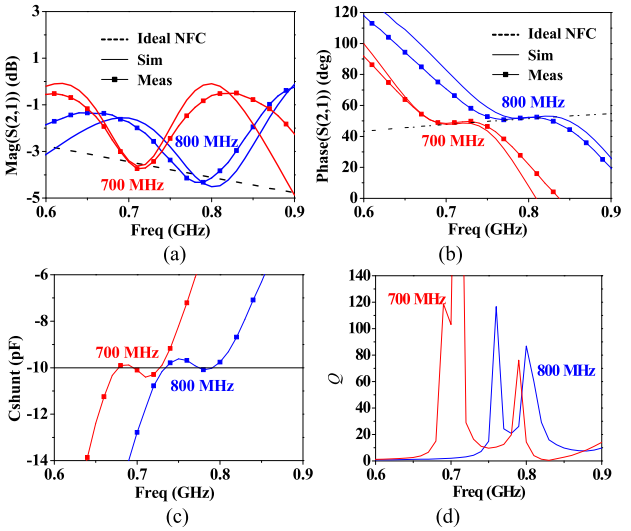

FIGURE 9. Experimental results of the reconfigurable 2nd order NFC circuit in shunt connection mode. (a) magnitude characteristic of S_{21}; (b) phase characteristic of S_{21}; (c) equivalent NF shunt capacitance calculated out from measured S_{21}; (d) Q factors.

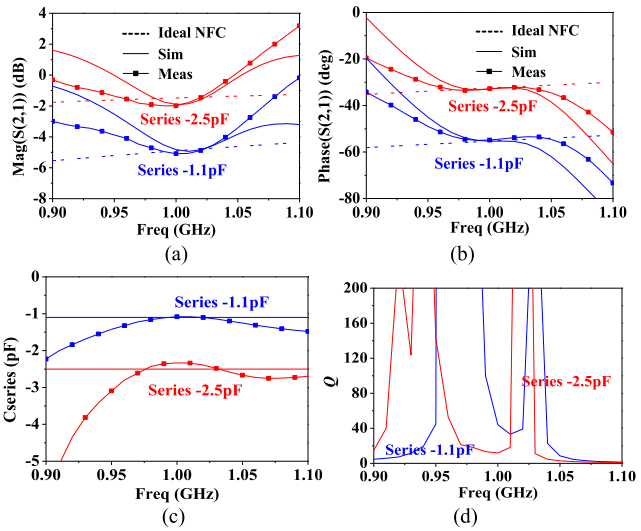

FIGURE 10. Experimental results of the reconfigurable 2nd order NFC circuit in series connection mode. (a) magnitude characteristic of S_{21}; (b) phase characteristic of S_{21}; (c) equivalent NF shunt capacitance calculated out from measured S_{21}; (d) Q factors.

the equivalent NFC value can be also flexibly controlled as will be demonstrated next section in series connection.

B. RECONFIGURABLE 2nd ORDER NFC CIRCUIT IN SERIES CONNECTION MODE

Fig. 10(a)(b) shows the simulated and measured results of the reconfigurable 2nd order NFC circuit in series connection mode. Simulation agrees well with the measurement. It can be seen that the measured *S*-parameter can be adjusted to match with −1.1 pF and −2.5 pF at the fixed center frequency 1 GHz. The equivalent series NFCs which are calculated from the *S*-parameter are shown in Fig. 10(c). It can be seen that the capacitance error is less than ±0.3 pF from 970 MHz to 1.02 GHz. The *Q* factors of different series capacitances are shown in Fig. 10(d), which are larger than 10. These experimental results demonstrate that the proposed NFC circuit can be equivalent to a series NFC with reconfigurable negative capacitive value. Note that the working frequency can be also controlled as have been demonstrated in shunt connection mode.

C. RECONFIGURABLE 2nd ORDER NFC CIRCUIT WITH SHUNT-TO-SERIES TRANSFORMATION

Fig. 11(a)(b) shows the simulation and measurement results of the reconfigurable 2nd order NFC circuit with shunt-to-series transformation. It can be seen that the reconfigurable transmission phase can cross 0° while keeping magnitude constant from 680 MHz to 730 MHz, indicating a transformation from series $-C$ of −10 pF to shunt $-C$ of −1.3 pF. Fig. 11(c) and (d) show the calculated NFCs and *Q* factors. It can be seen that the error is less than ±1 pF and *Q* is larger than 10. It proves the capability of shunt-to-series connection transformation for the proposed NFC circuit.

D. BANDWIDTH EXTENSION WITH A RECONFIGURABLE 3rd ORDER NFC CIRCUIT IN SHUNT CONNECTION MODE

The above-mentioned NFC's working bandwidth is narrow, typically less than 50 MHz. To increase the band-width, a 3rd order shunt NFC is fabricated and measured by introducing extra NGD cells.

TABLE 4. Comparisons with Previous works.

	Capacitance value reconfigurable	*Center frequency reconfigurable*	*Connection type reconfigurable*	*Capacitance value tuning range*	*Center Frequency tuning range*	*Q*
Ref. [13]	No	No	No	Fixed -2.4 pF	Fixed 1.2 GHz	>8
Ref. [25]	No	No	No	Fixed -5 pF	Fixed 2.5GHz	N/A
Ref. [27]	Yes	No	No	-0.5 pF to -1pF	Fixed 1.05GHz	N/A
Ref. [33]	No	No	No	Fixed -2 pF	Fixed 1.48GHz	>10
This work	Yes	Yes	Yes	-1.1 pF to -2.5pF (Frequency is fixed at 1 GHz)	0.7GHz to 0.8GHz (Capacitance is fixed at 10 pF)	>10

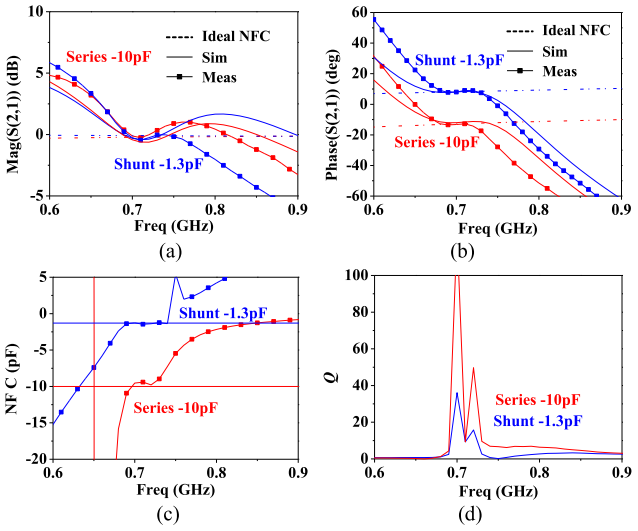

FIGURE 11. Experimental results of the reconfigurable 2nd order NFC circuit having capability of shunt-to-series transformation. (a) magnitude characteristic of S_{21}; (b) phase characteristic of S_{21}; (c) equivalent NF shunt capacitance calculated out from measured S_{21}; (d) Q factors.

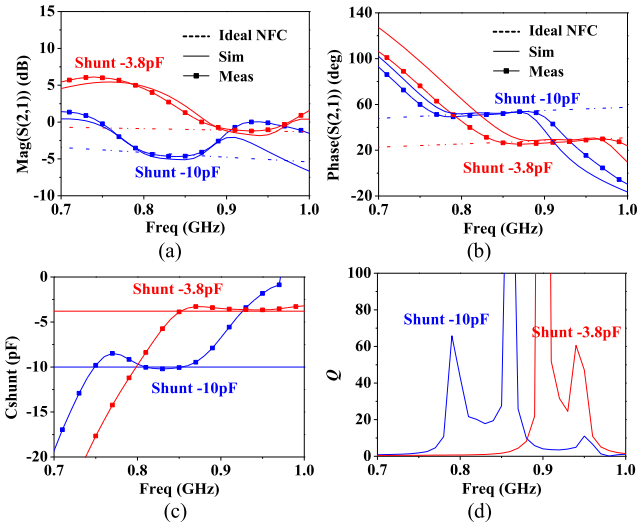

FIGURE 12. Experimental results of the reconfigurable 3rd order NFC circuit in shunt connection mode. (a) magnitude characteristic of S_{21}; (b) phase characteristic of S_{21}; (c) equivalent NF shunt capacitance calculated out from measured S_{21}; (d) Q factors.

Fig. 12(a) and (b) shows the simulation and experiment results of the 3rd order NFC circuit. It can be seen that the bandwidth is increased to 100 MHz from 780 MHz to 880 MHz, which is doubled as compared to the 2nd order NFC circuit given in Fig. 9. The center frequency of the proposed NFC can be tuned from 830 MHz to 940 MHz and the negative capacitance value can be tuned from -3.8 pF to -10 pF. Fig. 12(c) and (d) shows the calculated NFCs and Q factor. It can be seen that the error is less than ± 1 pF and Q is larger than 20.

Table IV gives the comparison with the previous works in literature. It can be seen that the proposed work has demonstrated the most flexible tuning capabilities that can have reconfigurable NFC value, reconfigurable working frequency and reconfigurable connection modes simultaneously. Moreover, the resultant NFC in this proposed work has highest Q value.

IV. CONCLUSION

In this paper, an N^{th} order distributed NGD circuit is studied to achieve a fully reconfigurable NFC. The adjustable transmission sections applying varactors are firstly studied to achieve the equivalent transmission lines with tunable characteristic impedance and phase. Using this structure, the gain, phase, and group delay response of the circuit can be consistent with an ideal NFC in a certain bandwidth. The proposed NGD circuit can accomplish the reconfigurable performance in capacitance value, working frequency and connection style at the same time or separately. Moreover, extra NGD cells can help to extend the effective bandwidth. Experiments have been given to verify the proposed theory.

REFERENCES

[1] L. Brillouin, *Wave Propagation and Group Velocity*. New York, NY, USA: Academic, 1960.
[2] G. Chaudhary, Y. Jeong, and J. Lim, "Miniaturized dual-band negative group delay circuit using dual-plane defected structures," *IEEE Microw. Wireless Compon. Lett.*, vol. 24, no. 8, pp. 521–523, Aug. 2014.
[3] G. Chaudhary, P. Kim, J. Kim, Y. Jeong, and J. Lim, "Coupled line negative group delay circuits with very low signal attenuation and multiple-pole characteristics," in *Proc. 44th Eur. Microw. Conf.*, Rome, Italy, 2014, pp. 25–28.
[4] Z. Wang, Y. Cao, T. Shao, S. Fang, and Y. Liu, "A negative group delay microwave circuit based on signal interference techniques," *IEEE Microw. Wireless Compon. Lett.*, vol. 28, no. 4, pp. 290–292, Apr. 2018.
[5] B. Ravelo, "Negative group-delay phenomenon analysis with distributed parallel interconnect line," *IEEE Trans. Electromagn. Compat.*, vol. 58, no. 2, pp. 573–580, Apr. 2016.
[6] T. Zhang, R. Xu, and C.-T. M. Wu, "Voltage-insensitive negative group delay circuit based on a stepped-impedance distributed amplifier," *IEEE Microw. Wireless Compon. Lett.*, vol. 27, no. 11, pp. 1007–1009, Nov. 2017.

[7] B. Ravelo, "Theory of coupled line coupler-based negative group delay microwave circuit," *IEEE Trans. Microw. Theory Techn.*, vol. 64, no. 11, pp. 3604–3611, Nov. 2016.
[8] C.-T. M. Wu and T. Itoh, "Maximally flat negative group-delay circuit: A microwave transversal filter approach," *IEEE Trans. Microw. Theory Techn.*, vol. 62, no. 6, pp. 1330–1342, Jun. 2014.
[9] C.-T. M. Wu, S. Gharavi, B. Daneshrad, and T. Itoh, "A dual-purpose reconfigurable negative group delay circuit based on distributed amplifiers," *IEEE Microw. Wireless Compon. Lett.*, vol. 23, no. 11, pp. 593–595, Nov. 2013.
[10] F. Wan, N. Li, B. Ravelo, J. Ge, and B. Li, "Time-domain experimentation of NGD activeRC-network cell," *IEEE Trans. Circuits Syst., II, Exp. Briefs*, vol. 66, no. 4, pp. 562–566, Apr. 2019.
[11] F. Wan, L. Wang, Q. Ji, and B. Ravelo, "Canonical transfer function of band-pass NGD circuit," *IET Circuits, Devices Syst.*, vol. 13, no. 2, pp. 125–130, Mar. 2019.
[12] F. Wan, N. Li, B. Ravelo, Q. Ji, B. Li, and J. Ge, "The design method of the active negative group delay circuits based on a microwave amplifier and an RL-series network," *IEEE Access*, vol. 6, pp. 33849–33858, 2018.
[13] M. M. Jacob and D. F. Sievenpiper, "Design, validation and trade-offs of non-foster circuits," in *IEEE MTT-S Int. Microw. Symp. Dig.*, Honolulu, HI, USA, Jun. 2017, pp. 344–347.
[14] A. A. Almahroug, A. P. Feresidis, and P. Gardner, "Non-Foster antenna matching networks using reflection-mode negative-group-delay networks," in *Proc. Loughborough Antennas Propag. Conf. (LAPC)*, Loughborough, U.K., Nov. 2016, pp. 1–4.
[15] Y. Wu, Z. Zhuang, H. Wang, and Y. Liu, "Impedance-transforming matched negative group delay circuits with enhanced bandwidth," in *Proc. IEEE Int. Workshop Electromagn., Appl. Student Innov. Competition (iWEM)*, Nanjing, China, May 2016, pp. 1–3.
[16] G. Chaudhary, Y. Jeong, and J. Im, "A design of reconfigurable negative group delay circuit without external resonators," *IEEE Antennas Wireless Propag. Lett.*, vol. 14, pp. 883–886, 2015.
[17] H. Mirzaei and G. V. Eleftheriades, "Unilateral non-Foster elements using loss-compensated negative-group-delay networks for guided- wave applications," in *IEEE MTT-S Int. Microw. Symp. Dig.*, Seattle, WA, USA, Jun. 2013, pp. 1–4.
[18] H. Mirzaei and G. V. Eleftheriades, "Realizing non-Foster reactances using negative-group-delay networks and applications to antennas," in *Proc. IEEE Radio Wireless Symp. (RWS)*, Newport Beach, CA, USA, Jan. 2014, pp. 58–60.
[19] Q. Tang and H. Xin, "Non-foster circuit for wideband matching of high frequency helical antenna," in *IEEE MTT-S Int. Microw. Symp. Dig.*, Honolulu, HI, USA, Jun. 2017, pp. 352–355.
[20] H. Mirzaei and G. V. Eleftheriades, "Arbitrary-angle squint-free beamforming in series-fed antenna arrays using non-foster elements synthesized by negative-group-delay networks," *IEEE Trans. Antennas Propag.*, vol. 63, no. 5, pp. 1997–2010, May 2015.
[21] W. Alomar and A. Mortazawi, "Elimination of beam squint in serially fed arrays with negative group delay circuits incorporating antenna elements," in *Proc. 42nd Eur. Microw. Conf.*, Amsterdam, The Netherlands, Oct./Nov. 2012, pp. 625–627.
[22] M. Jacob and D. Sievenpiper, "Gain and noise analysis of non-Foster matched antennas," *IEEE Trans. Antennas Propag.*, vol. 64, no. 12, pp. 4993–5004, Dec. 2016.
[23] D. S. Nagarkoti, Y. Hao, and K. Z. Rajab, "Radiation-Q bound of a small non-Foster antenna," in *Proc. IEEE Int. Symp. Antennas Propag. (APSURSI)*, Fajardo, Puerto Rico, Jun./Jul. 2016, pp. 187–188.
[24] N. Ivanov, V. Turgaliev, and D. Kholodnyak, "Performance improvement of an electrically-small loop antenna matched with non-foster negative inductance," in *IEEE MTT-S Int. Microw. Symp. Dig.*, Honolulu, HI, USA, Jun. 2017, pp. 348–351.
[25] S. Kolev, B. Delacressonniere, and J. L. Gautier, "Using a negative capacitance to increase the tuning range of a varactor diode in MMIC technology," *IEEE Trans. Microw. Theory Techn.*, vol. 49, no. 12, pp. 2425–2430, Dec. 2001.
[26] S. Lee, H. Park, J. Kim, and Y. Kwon, "A 6–18 GHz GaN pHEMT power amplifier using non-foster matching," in *IEEE MTT-S Int. Microw. Symp. Dig.*, Phoenix, AZ, USA, May 2015, pp. 1–4.
[27] Y. Song, S. Lee, E. Cho, J. Lee, and S. Nam, "A CMOS class-e power amplifier with voltage stress relief and enhanced efficiency," *IEEE Trans. Microw. Theory Techn.*, vol. 58, no. 2, pp. 310–317, Feb. 2010.
[28] S. Galal and B. Razavi, "40-Gb/s amplifier and ESD protection circuit in 0.18-μm CMOS technology," *IEEE J. Solid-State Circuits*, vol. 39, no. 12, pp. 2389–2396, Dec. 2004.
[29] N. Au and C. Seo, "A novel design of non-foster circuit using dispersive transmission line resonator," in *Proc. Int. Symp. Antennas Propag. (ISAP)*, Phuket, Thailand, Oct./Nov. 2017, pp. 1–2.
[30] M. Zhu and C.-T. M. Wu, "A tunable non-foster T-network loaded transmission line using distributed amplifier-based reconfigurable negative group delay circuit," in *Proc. Asia–Pacific Microw. Conf. (APMC)*, Kyoto, Japan, Nov. 2018, pp. 720–722.
[31] M. Zhu and C.-T. M. Wu, "A tunable series negative capacitor using distributed amplifier-based reconfigurable negative group delay circuit," in *Proc. 48th Eur. Microw. Conf. (EuMC)*, Madrid, Spain, Sep. 2018, pp. 616–619.
[32] A. Borjak, P. P. Monteiro, J. J. O'Reilly, and I. Darwazeh, "High-speed generalized distributed-amplifier-based transversal-filter topology for optical communication systems," *IEEE Trans. Microw. Theory Techn.*, vol. 45, no. 8, pp. 1453–1457, Aug. 1997.
[33] T. Zhang, C.-T. M. Wu, and R. Xu, "High Q series negative capacitor using negative group delay circuit based on a stepped-impedance distributed amplifier," *IEICE Electron. Express*, vol. 14, no. 7, 2017, Art. no. 20170088.